Universität Hamburg
DER FORSCHUNG | DER LEHRE | DER BILDUNG

Bachelorthesis

Chern-Numbers of the 1D-Heisenberg-Model

Jonah Fischer

jonah.fischer@studium.uni-hamburg.de
Studiengang B.Sc Physik
Matr.-Nr. 7263485

Erstgutachter: Professor M. Potthoff
Zweitgutachterin: Professor D. Pfannkuche

Abgabe: 02.11.2022

Abstract

The topological classification of a quantum system can lead to new and surprising physical phenomena such as the conducting edge states of a topological insulator or the quantization of the Hall conductance. The Chern number is a topological invariant which is useful for the characterization of such systems and their phases. For interacting spin systems these properties are still widely unknown. In this thesis we derive the topological phase diagram of the two-spin Heisenberg model, by computing the Chern numbers.

Zusammenfassung

Die topologische Klassifikation eines Quantensystems kann zu neuen physikalischen Phänomenen wie den leitenden Randzuständen eines topologischen Isolators oder der Quantisierung der Hall Leitfähigkeit führen. Die Chern-Zahl ist eine topologische Invariante, die zur Charakterisierung solcher Systeme und ihrer Phasen dienen kann. Für wechselwirkende Spinsysteme sind diese Eigenschaften noch weitgehend unbekannt. In dieser Arbeit untersuchen wir durch Berechnung der Chern-Zahlen das topologische Phasendiagramm des zwei-Spin Heisenberg Modells.

Hiermit versichere ich an Eides statt, dass ich die vorliegende Arbeit selbstständig und ohne fremde Hilfe angefertigt und mich anderer als der im beigefügten Verzeichnis angegebenen Hilfsmittel nicht bedient habe. Alle Stellen, die wörtlich oder sinngemäß aus Veröffentlichungen entnommen wurden, sind als solche kenntlich gemacht. Ich versichere weiterhin, dass ich die Arbeit vorher nicht in einem anderen Prüfungsverfahren eingereicht habe und die eingereichte schriftliche Fassung der auf dem elektronischen Speichermedium entspricht.
Ich bin mit einer Einstellung in den Bestand der Bibliothek des Fachbereiches einverstanden.

Hamburg, den 02.11.2022 Unterschrift: J. Fischer

Contents

1. Introduction

New materials with superior properties regarding stability, heat resistance or electrical conductance are indispensable in the improvement of already existing technologies and those ones which are still in development. The modification of materials with invasive methods, e.g, the doping of semiconductors, or external procedures, such as cooling a superconductor, can lead to surprising and fascinating physical phenomena. Such exotic states of matter can occur in various materials but are not always technically feasible. But as time goes on, problems get solved and the classification of theoretical states of matter can be relevant in future research. A rather new field of this kind of exotic states of matter are topological states.

The physics of topological states of matter and topological phase transitions is a highly topical and growing field in solid state physics. At the latest since 2016 it has received a lot of attention when D.J. Thouless, F.D.M. Haldane and J.M. Kosterlitz were awarded with the Nobelprize for their theoretical work on topological phases of matter. Topological states can be characterized by fundamental topological quantities that stay fixed under continuous transformations of system-dependent control parameters. These topological invariants define new topological phases of matter. These concepts found great success in the explanation of the quantum Hall effect (also known as the integer Hall effect) and recently for the discovery of topological insulators.

This bachelor thesis aims to classify the topological phases of the common quantum model for magnetism in solids - the Heisenberg model. Due to the complexity of interacting systems defined on $\mathcal{D}$-dimensional lattices, we will restrict our considerations to a very simple case - the Heisenberg model with two spin-1/2 lattice sites. Besides the exchange coupling J between the spins there are two external fields $\mathbf{B}_i$ each coupling to one of the spins. One static field and one with fixed modulus but arbitrary direction. The various directions of this second field form a closed two-dimensional parameter manifold with respect to which one can define a Chern number.

The thesis is organized as following:
The foundational theoretical concepts (Berry-phase, -curvature, Chern number and Heisenberg model) will be reviewed in section 2. Literature on the topics of sec. 2.1 can

be found in [5], sections 2.1.1-2.1.4 cover the concepts developed by M. Berry and the Chern number [1] [2]. The Heisenberg model is introduced in sec. 2.2 [4]. In sec. 2.3 a few cases are discussed that can be treated analytically [1]. A short overview on the python program coded for the numerical computations is given in section 3. Lastly, the numerically obtained results are presented and discussed in section 4.

2. Theoretical Background

2.1. Topology

Topology is a mathematical subject which deals with the geometrical properties of an object that are preserved under continuous deformations. This section shall give an overview over the concepts and mathematics of the topological properties of a quantum system. We start by reviewing a basic concept of topology. A mathematical object such as the surface of a sphere is called topologically equivalent to another object like the surface of a bowl, if it can be transformed into each other under a continuous deformation. In contrary to that we call two object topologically distinct if no continuous transformation exists. E.g. the surface of a torus is topologically distinct to the surface of a sphere, because it has a hole and there exists no smooth deformation to close it. On the other hand the torus can easily be deformed into other objects with exactly one hole, like a cylinder with open top/bottom surfaces or even a mug. The number of holes of a geometrical object is an example of an topological invariant. A topological invariant can not change under continuous transformations and therefore can characterize different objects into a single class.

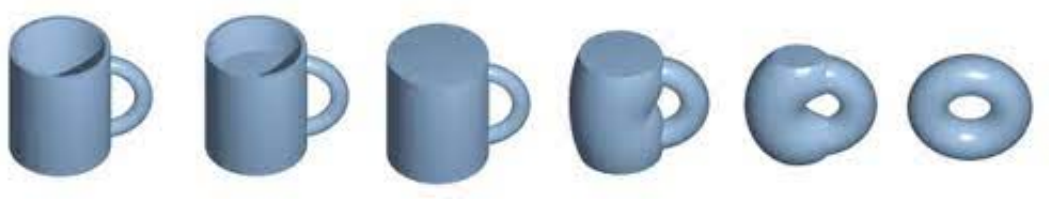

Figure 1: A mug can be transformed into a torus under a smooth deformation. The topological invariant "number of holes" stays fixed during the deformation - the objects are topologically equivalent. Image can be found in [11].

In recent research it became more clear that these topological concepts are not only of interest for mathematicians but can be applied to physical quantum systems. In the following sections we will introduce geometric properties of quantum states and a topological invariant which allows us to classify new (topological) phases.

2.1.1. Berry Phase

Consider a Hamiltonian $H(\mathbf{R})$ of a physical system that depends on some parameters $\mathbf{R} = (R_1, R_2, ..)$ which in turn are time dependent $R_i = R_i(t)$. With $\{|n(\mathbf{R}(t))\rangle\}$ being the eigenbasis of $H(\mathbf{R}(t))$ and $E_n(\mathbf{R}(t))$ the corresponding eigenvalues, we get:

$$H(\mathbf{R}(t))|n(\mathbf{R}(t))\rangle = E_n(\mathbf{R}(t))|n(\mathbf{R}(t))\rangle. \tag{1}$$

If at some time t_0 the system is in one of its eigenstates $|n(\mathbf{R}(t_0))\rangle$ and we slowly evolve the system Hamiltonian along a path C in the parameter space $[H(\mathbf{R}(t_0)) \to H(\mathbf{R}(t_1))]$, according to the adiabatic theorem [3], the system will stay in its instantaneous eigenstate $|n(\mathbf{R}(t_1))\rangle$.

When talking about the time evolution of our system, we also have to take the general time evolution of a quantum state into account. From basic quantum mechanics we know that a (time-independent) quantum state is evolving in time with the time evolution operator $U(t, t_0)$:

$$|n(t, \mathbf{R}(t))\rangle = U(t, t_0)|n(\mathbf{R}(t_0))\rangle = e^{-i\gamma(t,t_0)}|n(\mathbf{R}(t))\rangle. \tag{2}$$

Therefore our eigenstates are not only time dependent following their time dependency on $\mathbf{R}(t)$, but also accomplish a dynamical phase factor $\gamma(t, t_0)$ when evolving in time. In the same way we obtain the known result $e^{-i\gamma(t,t_0)} = e^{-iE_n(t-t_0)}$ for any time independent Hamiltonian $\tilde{H}$ by inserting their eigenstates $|\tilde{\psi}\rangle$ into the Schrödinger equation[1], we will do that for our $\mathbf{R}(t)$-dependent system:

$$H(\mathbf{R}(t))|n(t, \mathbf{R}(t))\rangle = i\frac{d}{dt}|n(t, \mathbf{R}(t))\rangle. \tag{3}$$

[1] This bachelor thesis is using the natural unit system with the constant $\hbar = 1$.

With eq. 1 and 3 we get:

$$\begin{aligned} E_n(\mathbf{R}(t))e^{-i\gamma(t,t_0)}|n(\mathbf{R}(t))\rangle &= e^{-i\gamma(t,t_0)}(\frac{d}{dt}\gamma(t,t_0))|n(\mathbf{R}(t))\rangle + ie^{-i\gamma(t,t_0)}\frac{d}{dt}|n(\mathbf{R}(t))\rangle \\ \Longleftrightarrow E_n(\mathbf{R}(t))|n(\mathbf{R}(t))\rangle &= (\frac{d}{dt}\gamma(t,t_0))|n(\mathbf{R}(t))\rangle + i\frac{d}{dt}|n(\mathbf{R}(t))\rangle. \end{aligned} \tag{4}$$

Taking the left-hand product with $\langle n(\mathbf{R}(t))|$ we further get:

$$\frac{d}{dt}\gamma(t,t_0) = E_n(\mathbf{R}(t)) - i\langle n(\mathbf{R}(t))|\frac{d}{dt}|n(\mathbf{R}(t))\rangle, \tag{5}$$

which leads us to:

$$\gamma(t,t_0) = \int_{t_0}^{t} E_n(\mathbf{R}(t'))\,dt' - i\int_{t_0}^{t}\langle n(\mathbf{R}(t'))|\frac{d}{dt'}|n(\mathbf{R}(t'))\rangle\,dt'. \tag{6}$$

The first term of eq. 6 is the already known dynamical phase and hence time dependent. On the other hand the second term is just dependent on the path C in the parameter space. In fact we can remove the explicit time-dependence from the integral completely:

$$\begin{aligned} \int_{t_1}^{t_2}\langle n(\mathbf{R}(t'))|\frac{d}{dt'}|n(\mathbf{R}(t'))\rangle\,dt' &= \int_{t_1}^{t_2}\langle n(\mathbf{R}(t'))|\nabla_{\mathbf{R}}|n(\mathbf{R}(t'))\rangle\frac{d\mathbf{R}}{dt'}\,dt' \\ &= \int_{\mathbf{R}(t_1)}^{\mathbf{R}(t_2)}\langle n(\mathbf{R})|\nabla_{\mathbf{R}}|n(\mathbf{R})\rangle\,d\mathbf{R}. \end{aligned} \tag{7}$$

This last expression of is now only dependent on the path C which starts at $\mathbf{R}(t_1)$ and ends at $\mathbf{R}(t_2)$. Therefore when evolving in time the quantum state obtains a purely geometrical phase - the so called Berry phase γ_n:

$$\gamma_n = i \int_C \langle n(\mathbf{R})|\nabla_{\mathbf{R}}|n(\mathbf{R})\rangle \, d\mathbf{R}. \tag{8}$$

Besides the Berry phase itself a closer look at the integrand can be interesting. This integrand denoted by

$$\mathcal{A}_n(\mathbf{R}) = i\langle n(\mathbf{R})|\nabla_{\mathbf{R}}|n(\mathbf{R})\rangle = -\mathrm{Im}\langle n(\mathbf{R})|\nabla_{\mathbf{R}}|n(\mathbf{R})\rangle. \tag{9}$$

is called the Berry connection (or sometimes the Berry potential) and is a gauge dependent vector valued quantity, making it an object similar to the vector potential in magnetostatics. For the second equality of eq. 9 we used $\nabla_{\mathbf{R}}\langle n(\mathbf{R})|n(\mathbf{R})\rangle = 0$ which means that $\langle n(\mathbf{R})|\nabla_{\mathbf{R}}|n(\mathbf{R})\rangle$ must be purely imaginary.

2.1.2. Gauge Dependence of the Berry-Phase and Berry-Connection

An important aspect to look at is the behaviour of the Berry phase under gauge transformations. When performing a gauge transformation $|n(\mathbf{R})\rangle \rightarrow e^{i\xi(\mathbf{R})}|n(\mathbf{R})\rangle$, $\xi(\mathbf{R})$ smooth, the Berry connection transforms as

$$\mathcal{A}_n(\mathbf{R}) \longrightarrow \mathcal{A}_n(\mathbf{R}) - \frac{\partial}{\partial \mathbf{R}}\xi(\mathbf{R}), \tag{10}$$

which leads to

$$\begin{aligned} \gamma_n = \int_C \mathcal{A}_n(\mathbf{R})\, d\mathbf{R} \longrightarrow \tilde{\gamma}_n &= \int_C \left(\mathcal{A}_n(\mathbf{R}) - \frac{\partial}{\partial \mathbf{R}}\xi(\mathbf{R})\right) d\mathbf{R} \\ &= \gamma_n - \Big(\xi(\mathbf{R}_2) - \xi(\mathbf{R}_1)\Big). \end{aligned} \tag{11}$$

With that in mind one could argue, that with the right choice of $\xi(\mathbf{R})$ the Berry phase could be cancelled and thus is not of relevance. This is true as long as the path C is an open path. When delimiting our choice of C on closed paths in the parameter space - $\mathbf{R}_1 = \mathbf{R}_2$, continuity demands that:

$$\xi(\mathbf{R}_2) - \xi(\mathbf{R}_1) = 2\pi m, \tag{12}$$

with $m \in \mathbb{Z}$.
We see that while the Berry phase factor $e^{-i\gamma_n}$ is independent of the chosen gauge, the Berry phase itself meets this condition only up to an integer multiple of 2π [1].

2.1.3. Numerical Calculation of the Berry-Phase and -Curvature

When computing the Berry phase and Berry connection numerically, the formulas 8 and 9 derived in section 2.1.1 are slightly inappropriate. They contain derivatives of our eigenstates and therefore analytical expressions of the eigenstates are required. Besides that, numerical diagonalization of the Hamiltonian will return the eigenstates with randomly different phase factors, so a gauge-independent formula is necessarry. Luckily, M. Berry provided an appropriate formula in his paper of 1984 [2], which can be derived using the Stokes theorem.
When focusing on closed paths in a 3-dimensional parameter space, we can apply the Stokes theorem to eq. 8 and get

$$\begin{aligned}
\gamma_n &= -Im \oint_C \langle n(\mathbf{R})|\nabla_{\mathbf{R}}|n(\mathbf{R})\rangle \, d\mathbf{R} \\
&= -Im \int_S \nabla_{\mathbf{R}} \times (\langle n(\mathbf{R})|\nabla_{\mathbf{R}}|n(\mathbf{R})\rangle) \, d\mathbf{S} \\
&= -Im \int_S \langle \nabla_{\mathbf{R}} n(\mathbf{R})| \times |\nabla_{\mathbf{R}} n(\mathbf{R})\rangle \, d\mathbf{S}.
\end{aligned} \tag{13}$$

Where S is the surface enclosed by C.

The expression $\mathbf{\Omega}_n(\mathbf{R}) = \nabla_{\mathbf{R}} \times A(\mathbf{R})$ is called the Berry curvature and will be the central quantity for the calculation of the Chern number (2.1.4).
With eq. 10 in mind we can think of $\mathbf{\Omega}_n(\mathbf{R})$ as some kind of magnetic field with $\mathcal{A}_n(\mathbf{R})$ as its vector potential. From this we can directely conclude that the Berry curvature has to be invariant under gauge transformations. By using that our eigenbasis $|n(\mathbf{R})\rangle$ represents a complete set of eigenstates, we can write

$$\mathbf{\Omega}_n(\mathbf{R}) = -\mathrm{Im} \sum_{n \neq m} \langle \nabla_{\mathbf{R}} n(\mathbf{R}) | m(\mathbf{R}) \rangle \times \langle m(\mathbf{R}) | \nabla_{\mathbf{R}} n(\mathbf{R}) \rangle, \tag{14}$$

and with the relation

$$\langle n(\mathbf{R}) | \nabla_{\mathbf{R}} m(\mathbf{R}) \rangle = \frac{\langle n(\mathbf{R}) | \nabla_{\mathbf{R}} H(\mathbf{R}) | m(\mathbf{R}) \rangle}{E_m(\mathbf{R}) - E_n(\mathbf{R})}, \tag{15}$$

this leads to

$$\mathbf{\Omega}_n(\mathbf{R}) = -\mathrm{Im} \sum_{n \neq m} \frac{\langle n(\mathbf{R}) | \nabla_{\mathbf{R}} H(\mathbf{R}) | m(\mathbf{R}) \rangle \times \langle m(\mathbf{R}) | \nabla_{\mathbf{R}} H(\mathbf{R}) | n(\mathbf{R}) \rangle}{(E_n(\mathbf{R}) - E_m(\mathbf{R}))^2}. \tag{16}$$

Eq. 16 can also be calculated componentwise using the Levi-Civita-tensor $\epsilon_{\alpha\beta\gamma}$ to remove the vectorproduct

$$\mathbf{\Omega}_{n,\alpha}(\mathbf{R}) = \frac{1}{2} \sum_{\beta\gamma} \epsilon_{\alpha\beta\gamma} \Omega_{\beta\gamma}(\mathbf{R}), \tag{17}$$

where

$$\Omega_{n,\beta\gamma}(\mathbf{R}) = -2 \, \mathrm{Im} \sum_{n \neq m} \frac{\langle n(\mathbf{R}) | \partial_\beta H(\mathbf{R}) | m(\mathbf{R}) \rangle \langle m(\mathbf{R}) | \partial_\gamma H(\mathbf{R}) | n(\mathbf{R}) \rangle}{(E_n(\mathbf{R}) - E_m(\mathbf{R}))^2}. \tag{18}$$

Eqs. 17 and 18 are the final formulas used for the numerical results of section 4. The representation of the Berry curvature as in eq. 15 shows that $\mathbf{\Omega}_n(\mathbf{R})$ is singular at points in the parameter space where degeneracies occur. In analogy to the Berry connection as a vector potential and the Berry curvature as some kind of field, these points behave like magnetic monopoles.

2.1.4. The Chern Number

With the considerations made in sec. 2.1.3 we are now able to define the central quantity of this bachelor thesis, namely the Chern number.
The Chern number is a topological invariant that can be defined for any quantum system as described above. In this bachelor thesis we will focus on the first Chern number[2] which is defined by

$$C = \frac{1}{2\pi} \oint_{\mathcal{S}} \mathbf{\Omega}_0(\mathbf{R}) \, d\mathbf{S}. \tag{19}$$

where $\mathbf{\Omega}_0(\mathbf{R})$ is the Berry curvature in terms of the ground state $|0\rangle$ and $\mathcal{S}$ is a closed surface embedded in a manifold[3] $\mathcal{M}$.
The Chern number is gauge invariant and most important integer valued. The property $C \in \mathbb{Z}$ makes the Chern number a quantity that is used to clearly distinguish different topological phases. A proof can be found in [8]. The gauge invariance of the Chern number is a consequence of the gauge invariance of $\mathbf{\Omega}_0(\mathbf{R})$.

The Chern number in a physical context is given by e.g. the quantum Hall effect dis-

[2] There are also Chern numbers of higher order which can be defined using calculus of differential forms. Higher Chern numbers exceed the content of this bachelor thesis and will not be discussed further.
[3] As before, now and following we will focus on a 3-dimensional parameter space $\mathcal{M}$

covered by K. von Kitzling et al. [6] and explained and connected to the Chern number by R.B. Laughlin [7] and D.J. Thouless et al. [10], [9]. In 1980 von Kitzling (Nobel prize 1985) discovered that the Hall conductance σ in a 2-dimensional electron gas is quantized by integer multiples of $\frac{e^2}{h}$, today known as the von Kitzling constant R_K:

$$\sigma = R_K m = \frac{e^2}{h} m. \tag{20}$$

A few years later these integer multiples were then identified as the first Chern numbers. This early work on the field of topological phases of matter was dealing with non interacting systems where the Berry phase is acquired by electrons on a path around the Brillioun zone which has the topology of a torus and the k-space (momentum space) is the parameter space.
However the Chern numbers investigated in this thesis will be computed for an interacting system with the parameter space given by an external field.

2.2. The Heisenberg Model

The study of collective magnetism in solids on a microscopic scale demands appropriate models, which can describe the known phenomena in an accurate and preferably simple way. Nowadays it is known that magnetism on a macroscopic scale is a result of the microscopic exchange interaction between localized spins. These local spins may result from an incompletely filled shell of the atoms forming the solid. A common and rather simple model for describing magnetism in solids is the Heisenberg-Model with its Hamiltonian given by eq. 21:

$$\begin{aligned} H &= -J \sum_{<i,j>}^{L} \mathbf{S}_i \mathbf{S}_j \\ &= -J \sum_{<i,j>}^{L} (\mathbf{S}_i^x \mathbf{S}_j^x + \mathbf{S}_i^y \mathbf{S}_j^y + \mathbf{S}_i^z \mathbf{S}_j^z) \\ &= -J \sum_{<i,j>}^{L} [\frac{1}{2}(\mathbf{S}_i^+ \mathbf{S}_j^- + \mathbf{S}_i^- \mathbf{S}_j^+) + \mathbf{S}_i^z \mathbf{S}_j^z]. \end{aligned} \tag{21}$$

The model describes the magnetic nearest neighbour interaction between the spins sitting on a linear lattice with L sites. The notation $< i, j >$ indicates that only interactions between nearest neighbours i and j is taken into account. The coupling constant J gives the strength of the interaction, while the sign of J determines either if the system is in ferromagnetic ($J < 0$) or in antiferromagnetic order ($J > 0$).

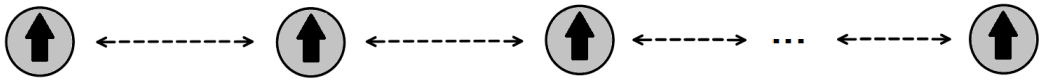

Figure 2: Sketch of a Heisenberg chain with L sites. The exchange interaction is given by J between the nearest neighbours. This example sketch shows a chain with open boundary conditions and a ferromagnetic coupling ($J < 0$), where the spins are aligned ferromagnetically (point in the same direction.)

The spins themselves are represented by the Spin vector $\mathbf{S} = (S_x, S_y, S_z)$. The last expression of eq. 21 is obtained by using the ladder operators

$$\mathbf{S}^+ = \mathbf{S}_x + i\mathbf{S}_y, \qquad \mathbf{S}^- = \mathbf{S}_x - i\mathbf{S}_y. \tag{22}$$

It is also possible to distinguish between periodic boundary conditions (PBC), meaning

that there is an interaction between the L-th spin and the first spin on the lattice, and open boundary conditions (OBC), where there is none.

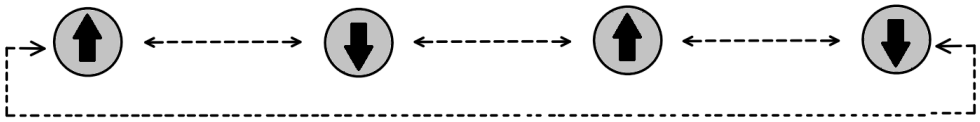

Figure 3: Sketch of a Heisenberg chain with $L = 4$ sites. Example with periodic boundary conditions (interaction between the fourth and the first spin) and antiferromagnetic coupling ($J > 0$).

2.2.1. The XXZ-Model

By choosing the coupling constant J to be direction-dependent, one can obtain the Hamiltonian of the so called Heisenberg-XXZ model given by:

$$H_{XXZ} = -\sum_{<i,j>}^{L} [\frac{J_{xy}}{2}(\mathbf{S}_i^+\mathbf{S}_j^- + \mathbf{S}_i^-\mathbf{S}_j^+) + J_z\mathbf{S}_i^z\mathbf{S}_j^z]. \tag{23}$$

This Hamiltonian represents a model where the interaction is equal in the x- and y-direction, but with a different couplingconstant J_z in the z-direction. By choosing a different coupling for the x- and y- direction as well, one could obtain another model, which would be called the Heisenberg-XYZ model.

2.2.2. External Field

The effective Hamiltonian we want to analyze in this bachelor thesis is given by:

$$H = H_{XXZ} - H_{\mathbf{B}} = -\sum_{<i,j>}^{L} [\frac{J_{xy}}{2}(\mathbf{S}_i^+\mathbf{S}_j^- + \mathbf{S}_i^-\mathbf{S}_j^+) + J_z\mathbf{S}_i^z\mathbf{S}_j^z] - \sum_{i}^{L} \mathbf{S}_i\mathbf{B}_i. \tag{24}$$

The extra term $H_{\mathbf{B}}$ represents external local magnetic fields $\mathbf{B}_i$, each acting (only) on the i-th spin. These magnetic fields $\mathbf{B}_i = (B_{x,i}, B_{y,i}, B_{z,i})$ now can serve as our set of control parameters for the adiabatic evolution:

$$\mathbf{R} = \{\mathbf{B}_i\}, \qquad i = 1, 2, ..., L. \tag{25}$$

For the computation of the Berry curvature and Chern number it is sufficient choose for example $\mathbf{R} = \mathbf{B}_1$ and let the remaining fields to be constant or 0 (no field). Thereby the parameter manifold $\mathcal{M}$ is fixed.

2.3. Analytical Considerations

2.3.1. Single Spin in a Magnetic Field

Before discussing the Heisenberg model we will quickly take a look at a model consisting of a single spin $\mathbf{S}$ in a magnetic field $\mathbf{B}$. The Hamiltonian of such system is given by

$$H = -\frac{1}{2}\mathbf{BS} = -\frac{1}{2}\begin{pmatrix} B_z & B_x - iB_y \\ B_x + iB_y & -B_z \end{pmatrix}. \tag{26}$$

The corresponding eigenenergies and eigenstates are then[4]

$$E_\pm = \pm\frac{1}{2}|\mathbf{B}| \tag{27}$$

$$|+\rangle = \begin{pmatrix} e^{-i\varphi}\sin(\frac{\theta}{2}) \\ \sin(\frac{\theta}{2}) \end{pmatrix}, \quad |-\rangle = \begin{pmatrix} e^{-i\varphi}\cos(\frac{\theta}{2}) \\ -\cos(\frac{\theta}{2}) \end{pmatrix}. \tag{28}$$

With eq. 13 the Berry curvature is then simply

[4]The eigenstates are given in spherical coordinates.

$$\mathbf{\Omega}_0(\mathbf{B}) = -\frac{1}{2}\frac{\mathbf{B}}{B^3} \tag{29}$$

When integrating over a closed surface that encloses the singularity at $\mathbf{B} = 0$ such as a sphere with radius $|\mathbf{B}|$ the first Chern number is obtained as

$$C = \frac{1}{2\pi}\oint_{\mathcal{S}} -\frac{1}{2}\frac{\mathbf{B}}{B^3}\, d\mathbf{S} = \pm\frac{1}{4\pi}4\pi = \pm 1, \tag{30}$$

depending on the orientation of $\mathcal{S}$.
This model is the example M. Berry discussed in 1984 [2] and can be found in most introductory papers and books on the topic [1]. The result we obtained here however is useful for testing the python program, as it is known and the single spin model can be considered a special case of the Heisenberg model if the magnetic field satisfies $B_i \gg J$.

2.3.2. Heisenberg Model for L = 2

We now take a look at the Heisenberg model for L = 2 (two spins) with magnetic field $\mathbf{B}_1$ and $\mathbf{B}_2$ coupled to the spins $\mathbf{S}_1$ and $\mathbf{S}_2$. The Hamiltonian of this system looks like

$$H = -J\mathbf{S}_1\mathbf{S}_2 - \mathbf{B}_1\mathbf{S}_1 - \mathbf{B}_2\mathbf{S}_2 \tag{31}$$

or in the matrix form

$$H = \begin{pmatrix} \frac{J}{4} - \frac{B_{z,1}}{2} - \frac{B_{z,2}}{2} & -\frac{B_{x,1}}{2} + i\frac{B_{y,1}}{2} & -\frac{B_{x,2}}{2} + i\frac{B_{y,2}}{2} & 0 \\ -\frac{B_{x,1}}{2} - i\frac{B_{y,1}}{2} & -\frac{J}{4} + \frac{B_{z,1}}{2} - \frac{B_{z,2}}{2} & \frac{J}{2} & -\frac{B_{x,2}}{2} + i\frac{B_{y,2}}{2} \\ -\frac{B_{x,2}}{2} - i\frac{B_{y,2}}{2} & \frac{J}{2} & -\frac{B_{x,1}}{2} + i\frac{B_{y,1}}{2} & -\frac{B_{x,1}}{2} + i\frac{B_{y,1}}{2} \\ 0 & -\frac{B_{x,2}}{2} - i\frac{B_{y,2}}{2} & -\frac{B_{x,1}}{2} - i\frac{B_{y,1}}{2} & \frac{J}{4} + \frac{B_{z,1}}{2} + \frac{B_{z,2}}{2} \end{pmatrix}. \tag{32}$$

Solving the eigenvalue problem for this matrix analytically is quite challenging and therefore numerical computations are required. For some special cases though it is possible to obtain analytical expressions for the energy levels in a simple form. For instance if we set the value of $\mathbf{B}_2$ to zero, the Hamiltonian simplifies and the energies are given by

$$\begin{aligned} E_0 &= \frac{1}{4}\Big(-J - 2\sqrt{J^2 + B_1^2}\Big) \\ E_1 &= \frac{1}{4}\Big(J - 2|B_1|\Big) \\ E_2 &= \frac{1}{4}\Big(J + 2|B_1|\Big) \\ E_3 &= \frac{1}{4}\Big(-J + 2\sqrt{J^2 + B_1^2}\Big) \end{aligned} \tag{33}$$

As already stated in sec. 2.1.3, we are interested in the points in the parameter space where degeneracies occur. For antiferromagnetic couplings $J > 0$, the ground state is always a singlet state and E_0 is the ground state energy. For ferromagnetic couplings $J < 0$, the ground state of the plain Heisenberg model ($\mathbf{B}_1 = \mathbf{B}_2 = 0$) is a triplet state with $E_0 = E_1 = E_2$ degenerate. These energy levels are shown in fig. 4 as a function of B_1 for a fixed ferromagnetic and antiferromagnetic coupling.

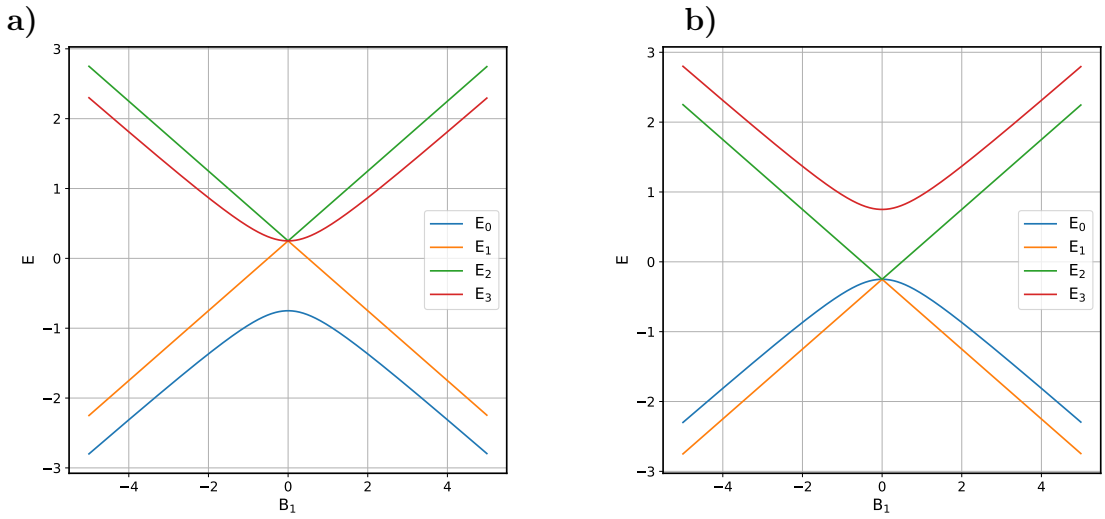

Figure 4: The energy levels E_0, E_1, E_2, E_3 as a function of B_1 for **a)** antiferromagnetic coupling $J = 1$ and **b)** ferromagnetic coupling $J = -1$. For antiferromagnetic couplings the ground state energy is always nondegenerate. For ferromagnetic couplings, the levels E_0, E_1 and E_2 cross at $B_1 = 0$. For $B_1 \neq 0$ the energy level E_1 defines the groundstate energy.

$B_1 < 0$ refers to the orientation of B_1 (or rather the orientation of the surface $\mathcal{S}$ defining B_1).
By setting the energy terms of eq. 33 equal we find:

$$\begin{aligned} E_0 &= E_1 \text{ for } J < 0 \wedge |B_1| = 0 \vee J = 0 \\ E_0 &= E_2 \text{ for } J \leq 0 \wedge |B_1| = 0 \\ E_0 &= E_3 \text{ for } J = 0 \wedge |B_1| = 0. \end{aligned} \tag{34}$$

The solution $J = 0 \wedge B = 0$ is the trivial result for a system with no interaction at all and therefore not of interest. The case $J < 0 \wedge B = 0$ means that the groundstate of the undisturbed ($B = 0$) ferromagnetic Heisenberg model is always triple degenerate. In fig. 5 these lines of degeneracy are shown in the parameter space.

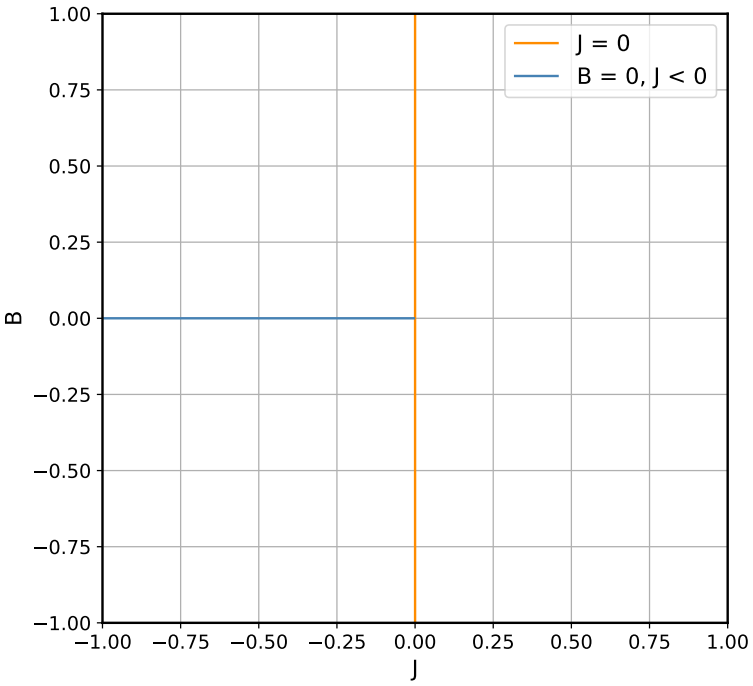

Figure 5: The "lines of degeneracy" in the parameter space for the L = 2 Heisenberg model with just a single external field B_1 acting on one of the spins.

3. Python Code

For a better understanding of how the results of sec. 4 were obtained, a quick overview of the python model is given here.
The first step was to code the Heisenberg model as given in eq. 24 and compute its matrix form for any parameters $L, J_{xy}, J_z, \mathbf{B}_i$. With the python library numpy then the eigenvalues and eigenstates where then obtained. Next the Berry curvature for every set of these parameters could be computed using formula 16. In the same way a set of Berry curvatures could be computed and then integrated by numerical integration to obtain the Chern number.

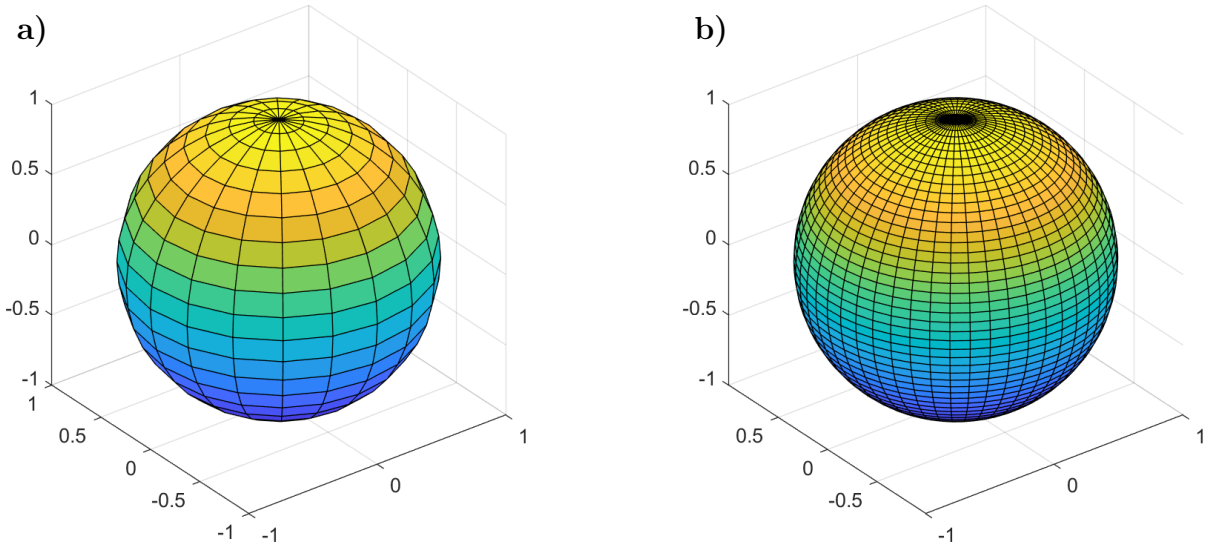

Figure 6: The surface $\mathcal{S}$ of a sphere lying in the 3-dimensional parameter space $\mathcal{M}$. **a)** parameterized by 20x20 descrete points and **b)** parameterized by 50x50 descrete points. The computed Chern numbers in sec. 4 where obtained by integrating over a sphere. (Plotted with MATLAB)

The surface $\mathcal{S}$ over which was integrated was that of a sphere. One of the magnetic fields acts as the parameter $\mathbf{R} = \mathbf{B}_i = (B_{i,x}, B_{i,y}, B_{i,z})$ that is integrated over the 2-sphere, while the other fields $\mathbf{B}_j$, $j \neq i$ remain static. Analogously the Chern numbers for various parameters $J_x y, J_z, \mathbf{B}_j$ could be computed and plotted into (topological) phase diagrams. The numerical integration works with discrete values of the integrand (Berry curvature) and the precision of the result is therefore dependent on the number

of values taken into account. The number of integrand values corresponds to the number of discrete points k^2 taken to parametrize the surface of the sphere. The surface of the sphere for two different parametrizations is shown in fig. 6.

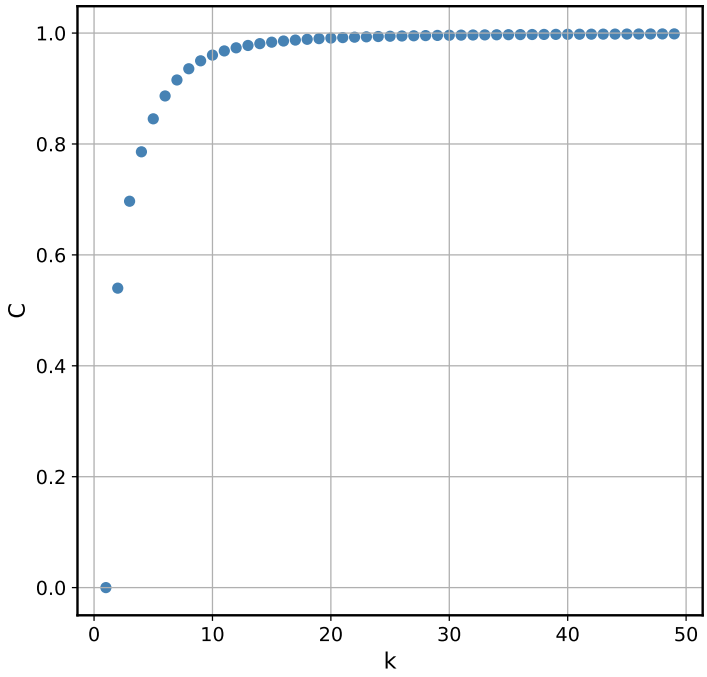

Figure 7: Integration accuracy of the Chern number as a function of k.

Fig. 7 shows the Chern number for a set of parameters as a function of k. For $k \longrightarrow \infty$ the graph would converge. After approximately $k \approx 20 \longrightarrow$ 20x20 parameterization points, the difference to the limit (actual Chern number) is of magnitude $\mathcal{O}(10^{-5})$. While the code produces reliable results, the computation takes rather long when taking more values for the integral. Therefore the results of sec. 4 where obtained with a parameterization of 20x20 points in parameter space. The usage of a more coarse parameterization of e.g only 10x10 parameterization points can lead to computational errors.

A phase diagram obtained with a parameterization of 10x10 parameterization points can be found in fig. 21 in appendix A.

4. Numerical Results

This section contains the results (phase diagrams and level crossing plots) numerically obtained with the python program. Although the program is able to build the Hamiltonian and compute the Chern numbers for Heisenberg chains with any number of sites/spins, we limit ourself to the simplest case - $L = 2$ sites. In such a system the parameters are J, B_1 and B_2, which can be varied independently.

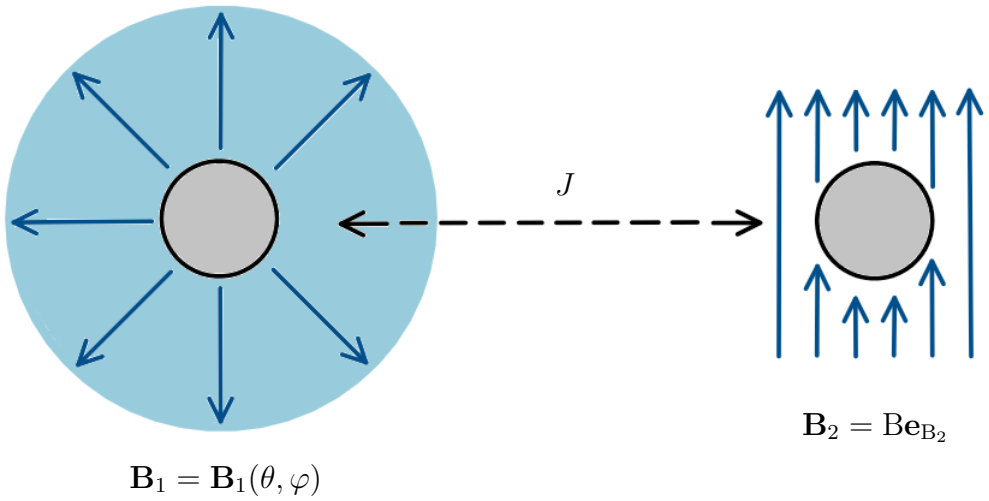

Figure 8: Sketch of a Heisenberg chain with two sites. The coupling J determines the exchange interaction between the spins. The field $\mathbf{B}_1(\theta, \varphi)$ acting on the first site serves as the control parameter $\mathbf{R}$ and takes values on the surface of a sphere. The field $\mathbf{B}_2$ acts on the second site and has a fixed orientation $\mathbf{e}_{B_2}$.

For all the results the field $\mathbf{B}_1$ will take parameters on the surface of a sphere when integrating over the Berry curvature. Changing the amplitude $|\mathbf{B}_1|$ then results in a change of the spheres radius. The second field $\mathbf{B}_2$ can change both in strength and direction. The coupling constant J can also change in its strength either as $J_{xy} = J_z = J$ or in case of a XXZ-model independently as J_{xy} and J_z.
By calculating the Chern number for different parameters J and $\mathbf{B}_i$ the different topological phases of the model could be classified.

4.1. XXX-Model $L = 2$, $\mathbf{B}_2 = 0$

We start by further investigating the model as considered in sec. 2.3.2. The magnetic field $\mathbf{B}_2$ acting on the second spin is set to zero. The Chern number then is a function

of J and $|\mathbf{B}_1|$ - $C = C(J, |\mathbf{B}_1|)$.

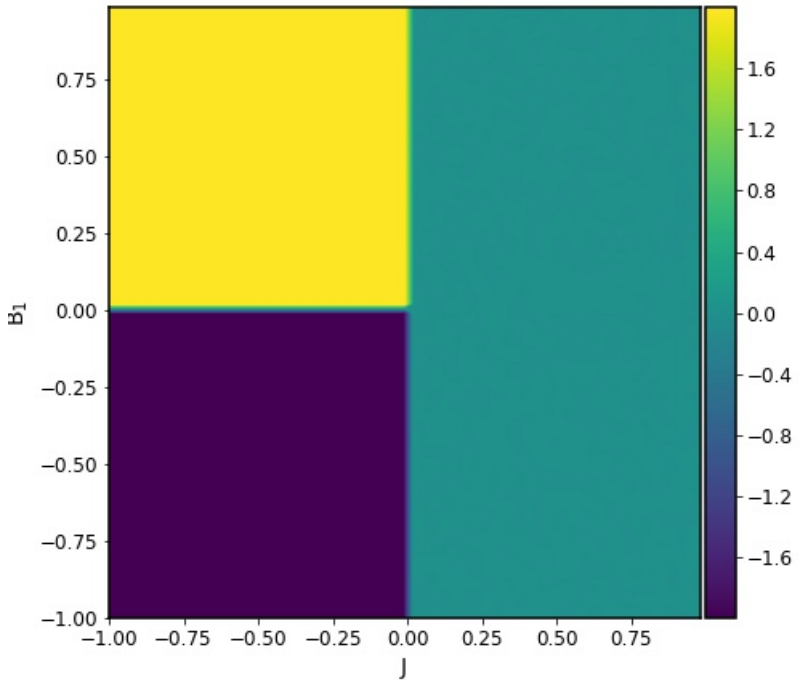

Figure 9: Topological phase diagram of the Heisenberg model with 2 spins and no static field $\mathbf{B}_2$ as a function of J and B_1: The value of the Chern number is given by the color coding. The yellow and the purple area represent different topological phases. The blue area at the right marks the (trivial) topological phase with $C = 0$. The blur at the edges is due to the numerical calculation.

The phase diagram represented in fig. 9 shows the topological phases for the $L = 2$ Heisenberg model with no static magnetic field ($\mathbf{B}_2 = 0$)[5]. The three different topological phases have the Chern numbers $C(J, |\mathbf{B}_1|) = 0, \pm 2$ and are separated by two straight lines. With the vertical line at $J = 0$ and the horizontal line located at $B = 0$ and $J < 0$ they match exactly with our "lines of degeneracy" discussed in sec. 2.3.2 and shown in fig. 5, making it a quite strong result validating the theory. For antiferromagnetic couplings there is only one phase with Chern number $C = 0$ (right side of the diagram). This can be understood by the absence of a level crossing of the groundstate energy with

[5]Technically the field was set to $B = 10^{-9}$ to break degeneracy a little. This was essential because we could not actually divide by zero.

the energy of an excited state for $J > 0$ (sec. 2.3.2).
The phases with Chern numbers $C = \pm 2$ occuring at ferromagnetic order, however were slightly unexpected. While the occurrence of two phases with reverse sign can be explained by the sign of $\mathbf{B}_1$ leading to reverse orientations of the surface's normal vector, the absolute value of 2 of the Chern number is not trivial. This value is probably originating from the triple degeneration for the plain ferromagnetic Heisenberg model ($B_1 = B_2 = 0$, $J < 0$).

4.2. XXX-Model $L = 2$, $\mathbf{B}_2 \neq 0$

We now compute the Chern number as a function of $|\mathbf{B}_1|$ and J with a static field $\mathbf{B}_2$ coupling to the second spin.

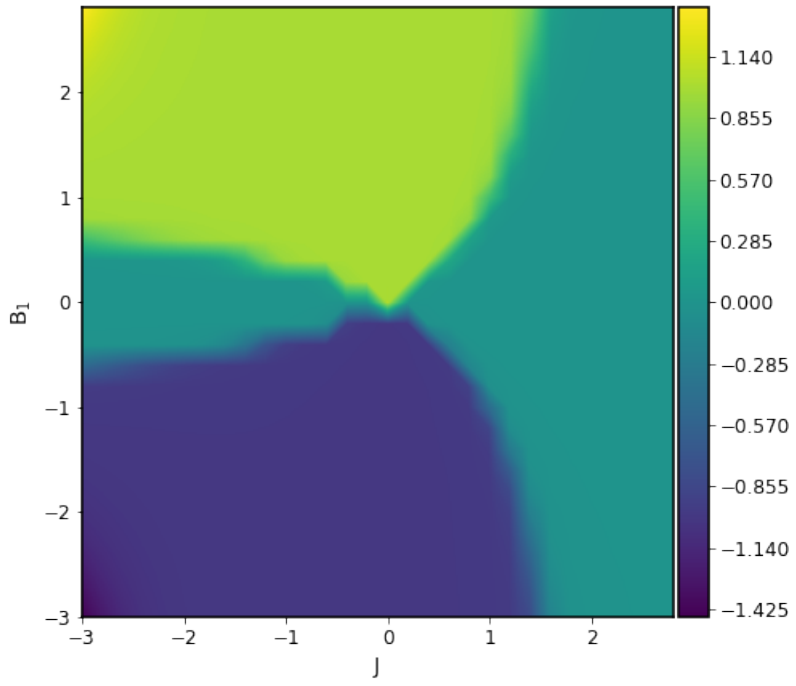

Figure 10: Topological phase diagram of the $L = 2$ XXX-model as a function of J and $|B_1|$. The amplitude of B_2 is fixed to $|B_{2,z}| = 1$.

Here we set $\mathbf{B}_2 = (0, 0, 1)$. The resulting phase diagram is shown in fig. 10. Unlike

fig. 9 there are now new topological phases with Chern number $C = \pm 1$ (green and darkblue). These phases originate at $J = 0$ for nonzero values of B_1 and are present in the ferromagnetic as well as the antiferromagnetic regime. Nonetheless for bigger antiferromagnetic ($J > 0$) values of the spin-coupling, a phase transition happens to the trivial phase with Chern number $C = 0$. In the ferromagnetic regime there is now also an area with Chern number $C = 0$. The trivial phase occurs only for small values of B_1 and seems to be less dependent on J as $|J|$ gets bigger (more negative). Also in the upper and lower left corner of the diagram in fig. 10 it seems that there is another not properly observable phase transition happening for values $B_1 > 3$ in the ferromagnetic regime.

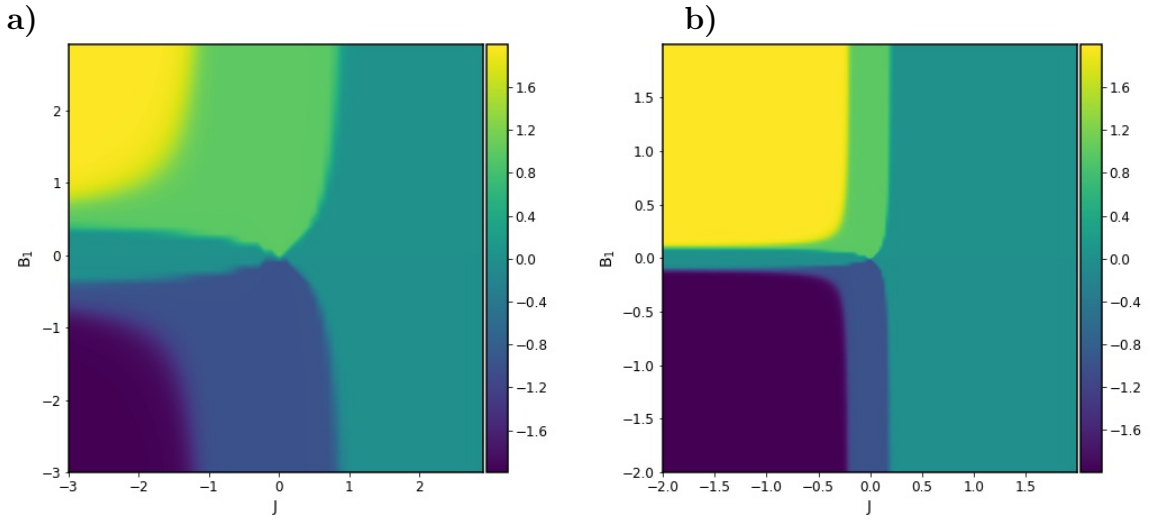

Figure 11: Phase diagrams with setting as in fig. 10 but with **a)** $|B_{2,z}| = 0.5$ and **b)** $|B_{2,z}| = 0.1$

The phase diagrams of fig. 11 where obtained similar to fig 10 but with smaller values of B_2. These phase diagrams now show clearly that there are more topological phases in the ferromagnetic regime. These phases have Chern number $C = \pm 2$ and occur for negative couplings $J < 0$ and nonzero fields B_1. When comparing figs. 11 a), b) and fig. 10 one can see that the phases with Chern number $C = \pm 1$ grow in size as B_2 gets bigger and are suppressed for small values of B_2. Further it seems that there are some critical values of J and B_1 at which the course of the phase edges stays constant. In other words e.g. in fig. 11 b) for $J \simeq 0.25$ and $B_1 \geq 0.1$ the phase transition $C = \pm 1 \longrightarrow C = 0$

happens regardless of higher values for $|B_1|$. The same behaviour can be observed for the transitions $C = 0 \longrightarrow C = \pm 1$ and $C = \pm 1 \longrightarrow C = \pm 2$.
With these observations in mind it is now also clear that for $B_2 = 0$ the phases with Chern number $C = \pm 1$ and the trivial phase in the ferromagnetic regime will vanish completely and the result of fig. 9 is obtained.

Instead of holding $\mathbf{B}_2 = (0, 0, B_z)$ constant, we can also fix the modulus of $\mathbf{B}_1$ and vary $B_{2,z}$.

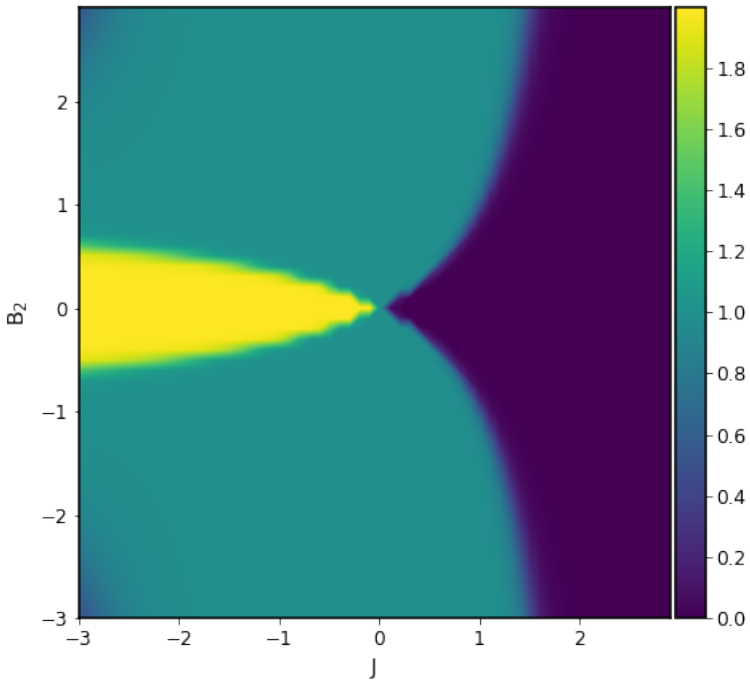

Figure 12: Topological phase diagram of the $L = 2$ XXX-model as a function of J and $B_{2,z}$. The modulus of B_1 is fixed to $|B_1| = 1$.

The phase diagram fig. 12 was obtained by integrating over a sphere with constant radius $|\mathbf{B}_1| = 1$ for various parameters J and $\mathbf{B}_2 = B_{2,z}$. There occur 3 different phases with Chern numbers $C = 0, 1, 2$. Due to the fixed positive orientation of the spheres normal vector, the sign of the Chern numbers is also positive. When taking smaller values for $|B_1|$ the phase diagrams shown in fig. 13 are obtained.

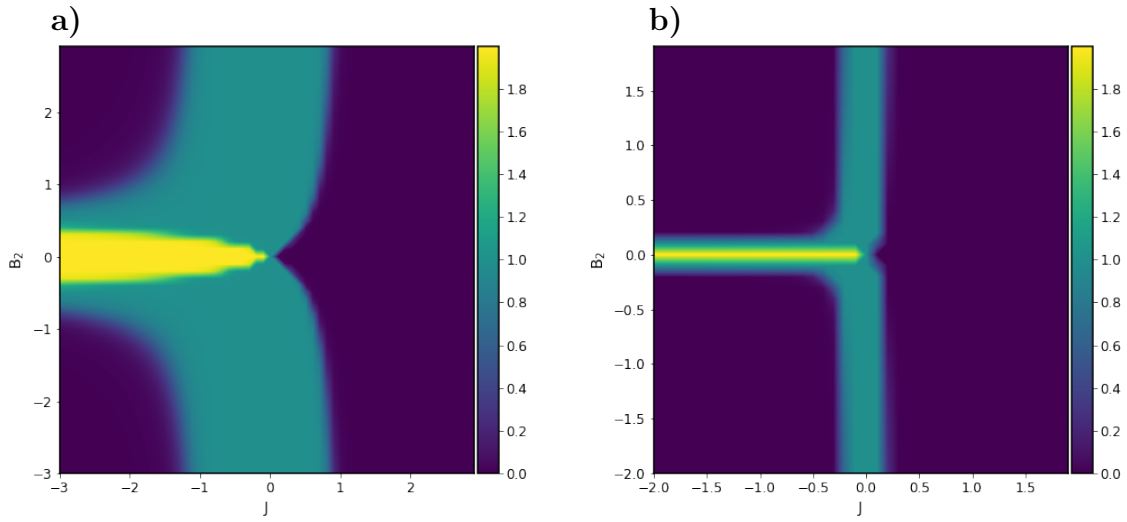

Figure 13: Phase diagrams with setting as in fig. 12 but with **a)** $|B_1| = 0.5$ and **b)** $|B_1| = 0.1$

These phase diagrams only refer to the same model but from a different perspective and therefore should be conform with the prior obtained results. Indeed, the phase diagrams have a similar form as the ones of fig. 10 and fig. 11, but with the phases of Chern number $C = 0$ and $C = \pm 2$ inverted in the ferromagnetic regime.

For this model of an $L = 2$ Heisenberg model with a nonzero field $\mathbf{B}_2$, the energy crossings between the groundstate and the excited states could not be calculated analytically. Nevertheless these degeneracies could be found numerically by plotting the minimum gap between the energy levels as a function of J and $\mathbf{B}_i$. These minimal gaps between the groundstate and the first excited state are plotted in fig. 14 b) for the parameters of fig. 13 b).

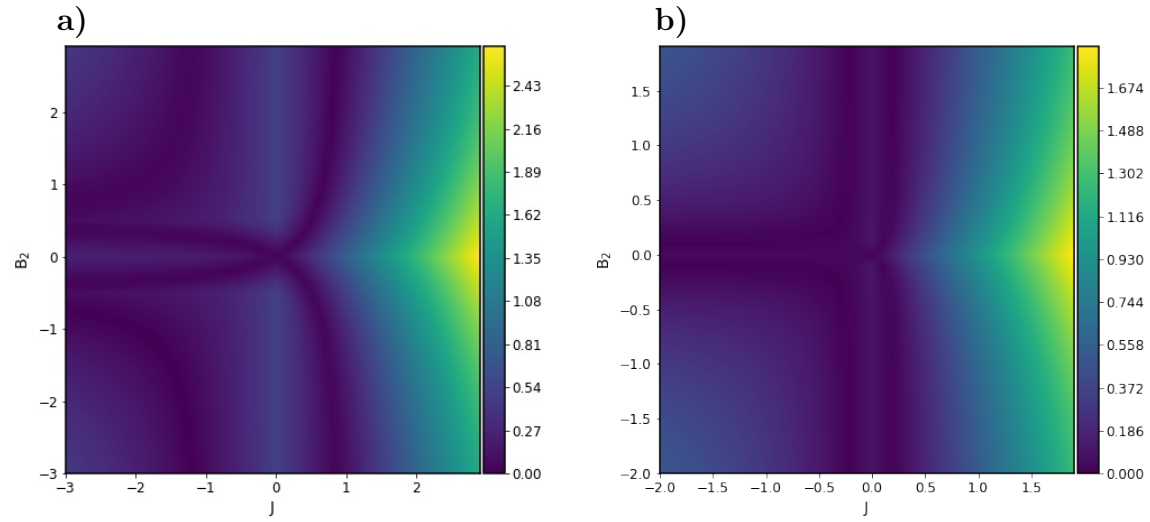

Figure 14: The minimal gap between the groundstate energy and the energy of the first excited state as a function of J and B_2 with **a)** $|B_1| = 0.5$ and **b)** $|B_1| = 0.1$

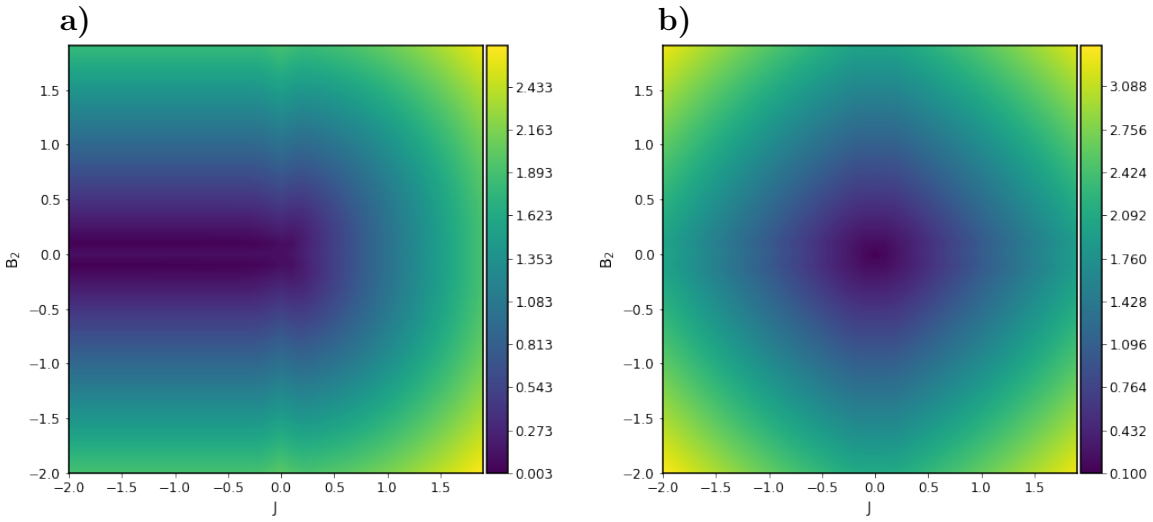

Figure 15: The minmal gap between the groundstate energy and the energy of the second and third excited states as a function of J and B_2 with $|B_1| = 0.1$ **a)** second excited state and **b)** third excited state

The dark purple curves in fig. 14 mark the points in parameter space where degeneracies occur. These curves follow the phase boundaries seen in fig. 13 and by that validate the results of the phase diagrams. It is interesting to point out, that the phase

transitions are only caused by degeneracies between the groundstate energy and the first excited state energy and not like in sec. 2.3.2, fig. 5 where there were also degeneracies between the ground state energy and the second excited state energy. This matter of fact can be shown by plotting the minimal gap between the groundstate energy and the energy of the second and third excited states (fig. 15). While the gap between the groundstate and the second excited state is very small (fig. 15 a)), it doesn't close. Meaning the topological phase transitions are only caused by gap closures between the ground state and the first excited state.

5. Discussion

5.1. Summary

In this bachelor thesis the theory of topological phases could be applied to the two spin Heisenberg chain. The Chern numbers could be computed for various settings of the parameters J, B_1 and B_2. For the Heisenberg XXX-model most of the topological phases transitions were found in the ferromagnetic regime.
For the simplest case with two coupled spins and only one external field $\mathbf{B}_1$ coupled to the first spin, three topological phases could be identified. The Chern numbers classifying these phases were found to be $C = 0, \pm 2$.
For the case of a second static field $\mathbf{B}_2$ coupled to the second spin, five topological phases with Chern numbers $C = 0, \pm 1, \pm 2$ were found. By studying this case for different strengths of $\mathbf{B}_2$ it could be shown, that the phases with Chern number $C = \pm 1$ occur in between the phase boundaries of fig. 9 and grow in size as a function of $\mathbf{B}_2$. By computing the minimal energy gap between the groundstate energy and the energies of the excited states the results could be validated.
Unfortunately the more complex case of the Heisenberg XXZ-model could not be classified. A phase diagrams obtained for XXZ-settings can be found in the appendix.

5.2. Outlook

For further research the topological classification of the XXZ-model could be of interest, as the direction dependency of the coupling constant has impact on the topological phases. A better understanding of the overall model can then be helpful in the classification of models with $L \geq 3$ spins. The python program coded for this thesis however is rather inefficient and has to be improved in terms of speed for the investigation of larger systems. A full classification of the Heisenberg model can also contribute to the classification of other models, as the Heisenberg model can be viewed at as the limit of the Hubbard model.

References

[1] B. Andrei Bernevig and Taylor L. Hughes. Topological insulators and topological superconductors. Princeton University Press, Princeton, 2013.

[2] M. V. Berry. Quantal Phase Factors Accompanying Adiabatic Changes. Proceedings of the Royal Society of London. Series A, Mathematical and Physical Sciences, 392(1802):45–57, 1984.

[3] M. Born and V. Fock. Beweis des Adiabatensatzes. Zeitschrift für Physik, 51(3):165–180, March 1928.

[4] Andreas Fledderjohann. Ground state properties of antiferromagnetic spin-1/2 Heisenberg systems in external fields. 2000. Bergische Universität Wuppertal.

[5] Marcel Franz and Laurens Molenkamp. Topological Insulators. Elsevier, 2013.

[6] K. v. Klitzing, G. Dorda, and M. Pepper. New Method for High-Accuracy Determination of the Fine-Structure Constant Based on Quantized Hall Resistance. Physical Review Letters, 45(6):494–497, August 1980.

[7] R. B. Laughlin. Quantized Hall conductivity in two dimensions. Physical Review B, 23(10):5632–5633, May 1981.

[8] M. Potthoff. Dynamical mean-field theory for correlated topological phases. In Lecture Notes of the Autumn School on Correlated Electrons 2022, 2022.

[9] D. J. Thouless. Quantization of particle transport. Physical Review B, 27(10):6083–6087, May 1983.

[10] D. J. Thouless, M. Kohmoto, M. P. Nightingale, and M. den Nijs. Quantized Hall Conductance in a Two-Dimensional Periodic Potential. Physical Review Letters, 49(6):405–408, August 1982.

[11] Russell Yang Qi Xun. *Emerging Scientists* Supplementary Issue II: Topological Circuits - A Stepping Stone in the Topological Revolution. Molecular Frontiers Journal, 04(Supp01):1–6, January 2020.

A. Appendix

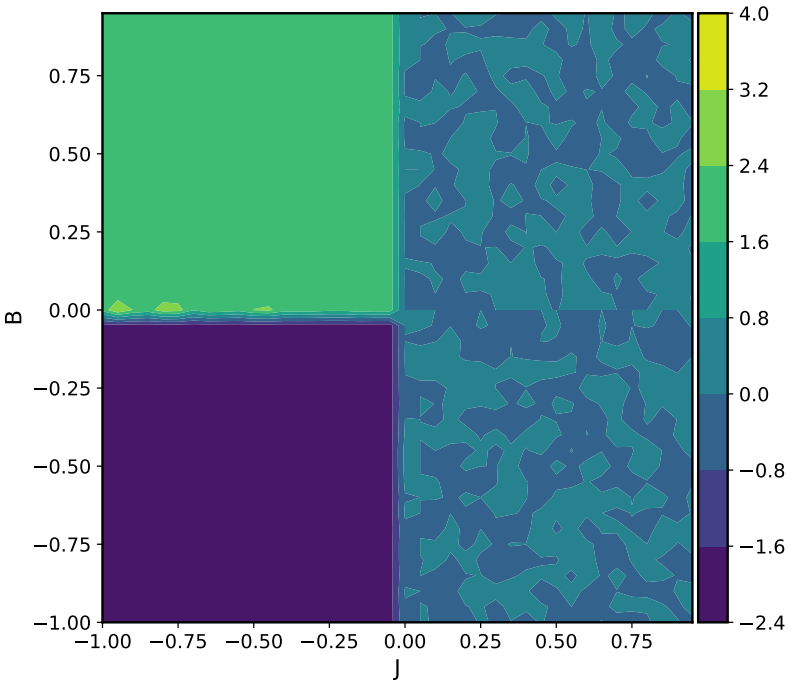

Figure 16: Phase diagram for the L = 2 Heisenberg model as a function of J and $|\mathbf{B}_1|$ and $B_2 = 0$ with a low integration accuracy. Due to the low accuracy the antiferromagnetic regime in the right area appears in two color gradings although only one phase with Chern number $C = 0$ occurs. In the ferromagnetic area, computation errors appear at the phase boundaries, resulting in higher Chern numbers, which in reality dont exist.

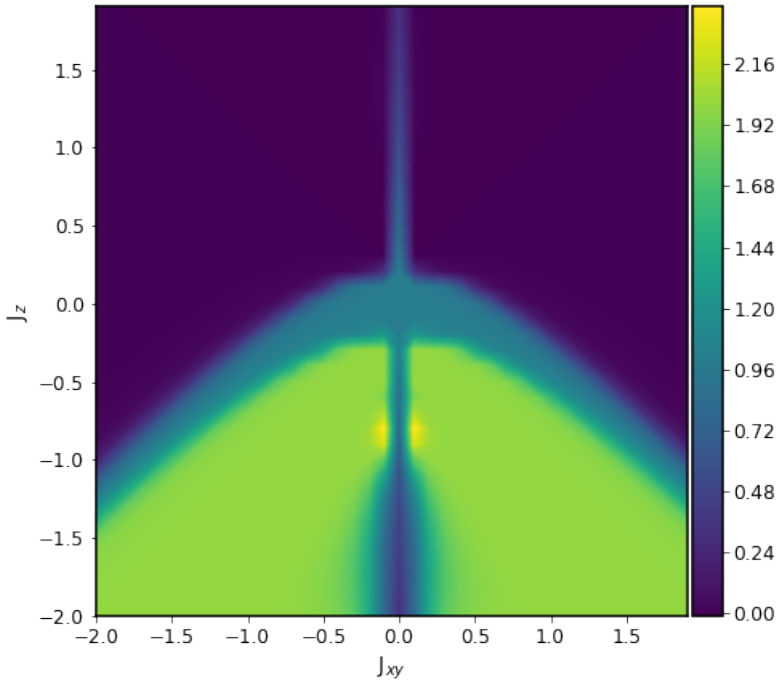

Figure 17: Phase diagram of the $L = 2$ Heisenberg XXX-model as a function of J_{xy} and J_z. $|\mathbf{B}_1| = 1$ and $\mathbf{B}_2 = B_{2,z} = 0.1$. Three topological phases with Chern numbers $C = 0, 1, 2$ were found. For positive (antiferromagnetic) couplings J_z the Chern number is $C = 0$ for most values of J_{xy}. Only around small values for J_{xy} the phase with Chern number $C = 1$ occurs. For ferromagnetic couplings J_z we observe a contrary behaviour. For most values of J_{xy} the Chern number is $C = 2$, while a transition to the phase with $C = 0$ occurs around $J_{xy} \approx 0$. Between the phases with Chern number $C = 0$ and $C = 2$, a transition to the phase with $C = 1$ happens. The small yellow areas around $J_z \approx -0.8$ and $J_{xy} \approx 0$ cannot be interpreted properly.

List of Figures